Functions of Fluctuation in the Heme-Binding Loops of Cytochrome b_5 Revealed in the Process of Heme Incorporation†

Masaki Ihara, Satoshi Takahashi, Koichiro Ishimori, and Isao Morishima*

Department of Molecular Engineering, Graduate School of Engineering, Kyoto University, Kyoto 606-8501, Japan

Received September 24, 1999; Revised Manuscript Received March 14, 2000

ABSTRACT: Cytochrome b_5 (cyt b_5) holds heme using two axial histidines, His63 and His39, that are located in the centers of the two heme-binding loops. The previous NMR study on the apo form of cyt b_5 (apocyt b_5) revealed that the loop including His63 exhibits a larger fluctuation compared to the other loop including His39 [Falzone, C. J., Mayer, M. R., Whiteman, E. L., Moore, C. D., and Lecomte, J. T. (1996) *Biochemistry 35*, 6519−6526]. To understand the significance of the fluctuation, the heme association and dissociation rates of the two loops were compared using two mutants of cyt b_5 in which one of the axial histidines was replaced with leucine. It was demonstrated that the fluctuating loop possesses a significantly slower heme dissociation rate and a faster heme association rate than the other loop. To further verify the importance of the fluctuating loop, the heme association process of wild-type apocyt b_5 was investigated using optical absorption and CD spectroscopies. It was indicated that the process proceeds through the two pathways, and that the dominant pathway involves the initial coordination of His63 located in the fluctuating loop. The urea concentration dependency of the rate constants revealed that the folding of the fluctuating loop is associated with the coordination of His63. It was suggested that the fluctuation enables the loop to have a larger heme−loop contact in the heme-bound conformation. The fluctuating heme-binding loops might be useful for the artificial design of heme-binding proteins.

One of the current challenges to researchers in the field of artificial design of proteins is to introduce heme-binding sites into a desired protein and to impart it with novel properties and activities. Since natural heme proteins perform a wide variety of biological activities, including oxygen binding and activation, electron transport, and signal transduction (*1*−*4*), the artificial design of heme-binding sites might lead to a strategy for constructing enzymes with various functions. DeGrado and his collaborators were the first who designed de novo heme proteins by introducing axial histidines or methionines inside the artificial helix bundles (*5*−*14*). They obtained proteins that can incorporate six-coordinate hemes using the designed residues. The designed heme proteins, however, always possess a marginal stability that is barely maintained by the coordination of two axial ligands to heme. The design of five-coordinate heme is currently impossible (*11*). As observed for cytochrome P450, natural heme proteins frequently use the open coordination site for the substrate binding and activation. The five-coordinate heme adjacent to the open pocket is necessary to attain the chemical activities of heme enzymes. Further developments in the artificial design of heme proteins require the investigation of the strategy taken by natural proteins to stabilize the heme binding.

The stability of the heme protein association can be defined as the difference in the Gibbs free energies of the protein in the heme-bound (holo) state and in the heme-free (apo) state. Accordingly, the structural properties of heme proteins both in the holo and apo forms are important for the understanding of the stability. Only three heme proteins (myoglobin, cytochrome b_5, and cytochrome b_{562}) have been characterized structurally in both their holo and apo forms. It is clarified that all three proteins in their apo forms highly maintain the holo-like structures except for some conformational fluctuations observed in the localized regions, including the axial ligands of the heme (*15*−*25*). In the case of apomyoglobin, a loop containing the proximal histidine experiences the conformational fluctuation (*15*−*18*). The solution structures of apocytochromes b_5 and b_{562} show the significant structural fluctuations in one side of the heme-binding sites (*19*−*21*, *24*, *25*). The importance of the fluctuating regions for the stable heme binding has also been noticed through the efforts in the artificial design of heme proteins. Choma et al. (*5*) observed that a relatively stable heme−bundle complex was obtained when the bundle structure in the absence of heme was made intentionally destabilized rather than fixed, and suggested that the fluctuation in the apo structure of the designed protein might help to attain a stable conformation in the holo form. While it is sometimes assumed that local fluctuation of proteins is related to the binding of the substrate, DNA, and antigen (*24*−*28*), little is known about its significance for the heme binding. In this article, we intend to clarify the functions of fluctuating heme-binding loops commonly observed in the natural and artificial heme proteins.

† This work was supported by grants-in-aid for scientific research on priority areas Molecular Biometallics (08249102 to I.M.) and Principles of Protein Architecture (07280101 to K.I.) from the Ministry of Education, Science, Culture and Sports.

* To whom correspondence should be addressed. Telephone: (81)-75-753-5921. Fax: (81)-75-751-7611. E-mail: morisima@mds.moleng.kyoto-u.ac.jp.

10.1021/bi9922289 CCC: $19.00
Published on Web 04/29/2000

As the target of investigating the functions of the fluctuating loops observed in the heme-binding proteins, we focused on cytochrome b_5 (cyt b_5).[1] The protein has ca. 90 amino acid residues and serves to transport electrons in hepatic endoplasmic reticulum and erythrocytes (*29*−*32*). The three-dimensional structures of the soluble fragment of cyt b_5 determined by X-ray crystallography (*33*, *34*) and ^{1}H NMR spectroscopy (*35*−*39*) revealed that the heme site is six-coordinate and situated inside the four-helix bundle. The two axial histidines, His39 and His63, are located in the centers of the two helix−turn−helix loops. While the two loops in the holo form are stable and possess very similar conformations, including the locations of the axial histidines and nearby phenylalanines, they experience rather different environments in the apo form (*24*, *25*). The extensive NMR studies on apocyt b_5 revealed that the region between Ala50 and Glu69, which includes the axial His63, exhibits a large fluctuation, while the region around the other histidine (His39) forms a relatively stable conformation (*24*, *25*). The presence of the two loops having similar conformations in the holo form but different fluctuations in the apo form makes the protein an ideal target for investigating the functions of the fluctuating loops. By comparing the properties of the two loops, we expect to clarify the implication of the fluctuations.

We investigated the kinetics of the heme association and dissociation of cyt b_5, and estimated the equilibrium constants of the heme association from comparison of the both rate constants. To differentiate the functions of the two loops, we constructed two mutants of cyt b_5 in which one of the axial histidines was substituted for a leucine residue (H63L and H39L). Since the substitutions abolish the heme binding property of one of the loops, the heme association and dissociation kinetics of the mutants would reflect the properties of the remaining heme-binding loops. The process of the heme incorporation of wild-type cyt b_5 was also analyzed to confirm the functions of the two loops. The spectroscopic properties of the mutants allowed us to identify the first histidine that coordinates to the heme during the heme incorporation process of the wild-type protein. Our results clearly indicate that the fluctuating heme-binding loop containing His63 has a higher affinity for heme than the other loop containing His39.

EXPERIMENTAL PROCEDURES

Site-Directed Mutageneses. Site-directed mutageneses were carried out by using the polymerase chain reaction technique. Two synthetic oligonucleotides, 5′-TTCGCCAC-CTGGCAGCTCTTCGAGGA-3′ and 5′-CGTCGGTACT-CAGGCCAACGTCT-3′, were used as primers to multiply the double-stranded DNA fragments and to introduce mutations His39 → Leu and His63 → Leu, respectively. The mutated fragments were ligated into the pUC13 plasmid (*40*) at the unique *Pst*I and *Eco*RI restriction sites. The introductions of the mutations were verified by using a DNA sequencer (model 373, Applied Biosystems).

Expression and Purification of Proteins. A rat hepatic cytochrome b_5 whose C-terminal membrane binding domain was deleted was used as the wild-type protein. Wild-type cyt b_5 was expressed in *Escherichia coli* strain TB1 and purified as previously described (*40*). In brief, the cells grown overnight were harvested and lysed. After removal of cell debris by centrifugation, the supernatant was purified using DEAE-Sephacel and Sephadex G-50 columns until the A_{412}/A_{280} ratio (RZ value) exceeded 5.5 and a single band was observed for the purified sample on SDS-containing gels.

Since the two cyt b_5 mutants failed to incorporate heme in vivo and were sensitive to protease digestions, they were transformed into the protease-deficient strain of *E. coli*, BL21(DE3). Furthermore, all the buffer solutions used in the purification steps contained 10 mM PMSF and 5 mM EDTA for inhibition of protease activities. The supernatant of lysed cells was applied to a DEAE-Sephacel column equilibrated with 50 mM Tris-acetate buffer at pH 8.0 and washed with the same buffer until the absorbance of the elution at 260−280 nm was diminished. The protein was eluted with a KCl gradient from 0 to 300 mM. Fractions containing cyt b_5 were collected and dialyzed against 100 mM sodium phosphate buffer at pH 7.5 and applied to a DEAE-Sephacel column equilibrated with the same buffer. The gradient of KCl from 0 to 300 mM was again used to elute the purified protein. The apoprotein was concentrated and passed through a Sephadex G-50 column equilibrated with 50 mM Tris-acetate buffer at pH 8.0 several times. Finally, a slight excess of hemin dissolved in a 0.1 N NaOH solution was added to the apoprotein solution. The reconstituted proteins were purified by using Sephadex G-25 and G-50 columns equilibrated with 50 mM Tris-acetate buffer at pH 8.0. The typical yield of the purified mutants was about 100 mg from 18 L of culture.

Spectroscopic Measurements. The static electronic absorption spectra of the purified proteins (5−7 μM) at 25 °C in 100 mM sodium phosphate buffer (pH 8.0) were recorded on a UV−visible spectrophotometer (UV-2200, Shimadzu). Extinction coefficients were calculated from the heme content determined by the pyridine−hemochromogen assay (*41*).

The static CD spectra of the purified proteins in the Soret region were measured at 25 °C on a spectropolarimeter (J-720, Jasco). The sample concentration was 5 μM in 100 mM sodium phosphate buffer at pH 8.0. The path length of the cells used for the static measurements was 10 mm. The spectra were the averages of 10 scans recorded at a speed of 100 nm/min with a resolution of 0.2 nm.

Kinetic Measurements of Heme Incorporation. The heme incorporation reactions were initiated by rapidly mixing the apoprotein and cyanohemin solutions using a stopped-flow mixer (Unisoku). The kinetic absorption spectra were obtained at 25 °C using a rapid-scan monochromator (RSM-1000, Olis) that was connected to the mixer using optical fibers. The transient CD spectra were obtained at 25 °C by manually mixing the protein and hemin solutions in a cell whose path length was 40 mm. The kinetic absorption and CD spectra were analyzed using a least-squares fitting subroutine of Mathcad (Mathsoft). Igor-Pro (Wavemetrics) was used for the data presentation.

An appropriate amount of hemin was first dissolved in a 0.1 M solution of NaOH and diluted with 100 mM phosphate buffer containing NaCN (pH 8.0). All hemin solutions were used within 5 h of preparation. Apocyt b_5 was prepared by the method of Teale (*42*). Typically, 100 nmol of cyt b_5 in

[1] Abbreviations: cyt b_5, cytochrome b_5; CD, circular dichroism; NMR, nuclear magnetic resonance; ASA, solvent accessible surface area.

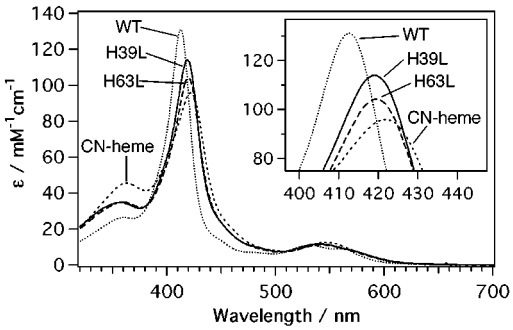

FIGURE 1: Electronic absorption spectra for H63L (− − −), H39L (—), wild-type cyt b_5 (•••), and dicyanohemin (- - -). The buffer solutions of the mutants and dicyanohemin contained 15 mM NaCN. The inset shows the expansion of the Soret region.

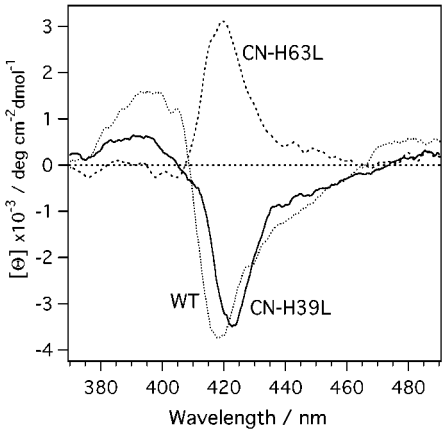

FIGURE 2: CD spectra in the Soret region for H63L (- - -), H39L (—), and wild-type cyt b_5 (•••). The buffer solutions of the mutants contained 15 mM NaCN.

5.0 mL of 100 mM sodium phosphate at pH 7.0 was brought to pH 2.0 by slowly adding 2.0 N HCl at 0 °C. An equal volume of cooled 2-butanone was added to the protein solution and mixed. The organic layer containing heme was removed. The procedure was repeated several times until the organic layer turned colorless. The aqueous solution containing apoprotein was dialyzed for 24 h against 20 mM sodium phosphate buffer containing 0.2 mM EDTA (pH 8.0). The concentrations of wild-type and mutant apocyt b_5 were estimated by using an ϵ_{280} of 10.5 mM^{-1} (*43*).

Measurements of the Rate of Heme Dissociation from the Cyt b_5 Mutants. The rates of heme dissociation from the cyt b_5 mutants were analyzed using the method described by Qian et al. (*44*). Heme extraction reactions from the mutant cyt b_5s (1.5 μM) to the excess amount of apomyoglobin (50 μM) were monitored at 427 nm in 0.1 M sodium phosphate buffer (pH 8.0) at 15 °C. The sample solution contains 0.45 M sucrose to stabilize the apomyoglobin (*45*). Since the apparent rate constants for heme extraction (k_{obs}) observed at 50 and 100 μM apomyoglobin were the same, we consider the observed rate constants (k_{obs}) identical with the rate constants for the heme dissociation (k_{-H}) from the mutants.

RESULTS

Spectroscopic Properties of Wild-Type and Mutant Cyt b_5s. We replaced one of the axial histidines with leucine to construct two axial mutants of cyt b_5, H39L and H63L. To understand the structural properties of the constructed mutants, we first investigated their spectroscopic properties. As shown in Figure 1, the electronic absorption spectra of the mutants in the presence of cyanide are distinguished from those of wild-type cyt b_5 and dicyanohemin. The peak positions of the both mutants are at 419 and 540 nm, which are similar to those of cyanometmyoglobin at 422 and 540 nm, respectively, indicating that the coordination structures of the mutants are the CN-His type. It should be noted that the electronic absorption spectra for the cyanide-bound form of H39L and H63L are slightly different from each other as shown in the inset of Figure 1. The lower Soret intensity of H63L suggests the existence of a small amount of free hemin.

Soret CD spectra of heme proteins reflect the distributions of aromatic residues around the heme (*46*). The CD spectra for wild-type cyt b_5 in the oxidized form and for the cyanomet H39L mutant (CN-H39L) are presented in Figure 2, showing negative maxima at 418 and 423 nm, respectively. On the other hand, the cyanomet H63L mutant (CN-H63L) has a positive maximum at 420 nm (Figure 2). Since dicyanohemin in solution and hemin attached on the surface of proteins afford no optical ellipticity (data not shown), the appearance of the optical ellipticity for both of the mutants indicates that the heme is incorporated inside the heme pocket. We conclude that the heme−H39L complex possesses cyanide and His63 as the axial ligands, and that the heme−H63L complex possesses cyanide and His39.

Heme Incorporation and Dissociation Rates of Mutant Cyt b_5s. To evaluate the properties of each heme-binding loop, the kinetic rates of the heme association with the mutant cyt b_5s were estimated. Apo mutants at concentrations of 5, 10, and 15 μM were mixed with 1 μM dicyanohemin in the presence of 25 mM cyanide at pH 8.0. The reactions of 5 μM apo mutants and 1 μM dicyanohemin were also carried out in the presence of 15, 25, and 35 mM cyanide at pH 8.0. The resultant rapid-scan spectra for all the experiments exhibit clear isosbestic points, and the absorption changes measured at 419 nm exhibited single-exponential curves (data not shown). These observations indicate that the process can be described as a two-state reaction. The apparent rate constants of the heme association are linearly dependent on the apoprotein concentration and on the inverse of the cyanide concentration. The association rate constants are 2.7 ± 0.2 and 1.5 ± 0.06 mM^{-1} s^{-1} for H39L and H63L, respectively. The cyanide concentration dependency suggests that the first step of the heme incorporation process should be the coordination of the axial histidine of apoprotein to monocyanohemin which is in equilibrium with dicyanohemin.

The faster heme association with H39L might be explained by the difference in the ionization constants of the axial histidine residues. To examine the effect of the possible difference in pK_a, we conducted the heme association reactions at the elevated pH (pH 9.0). The ratios of the observed association rates for the two mutants (k_{H39L}/k_{H63L}) are 1.8 and 1.6 at pH 8 and 9, respectively. The invariance of the ratio indicates that both axial residues are fully deprotonated at pH 8.0. We conclude that the faster association of H39L is not due to the difference in the ionization states of the axial histidines.

Heme dissociation rates from the holoproteins have been used to evaluate the affinities between heme and apoproteins (*44*, *45*, *47*−*49*). The Soret absorption maxima of the two

mutants in the cyanide-bound form were observed at 419 nm (Figure 1), which are distinct from that of wild-type Mb (422 nm). We can, therefore, monitor spectroscopically the transfer of heme from the mutants to the excess amount of apomyoglobin in the presence of cyanide. The time courses were measured at 427 nm which corresponds to the maxima of the difference spectra between the CN-bound mutants of cyt b_5 and CN-bound myoglobin. In the case of CN-H39L, the kinetic trace of the absorption change at 427 nm exhibited a single-exponential curve (data not shown). The apparent rate constant [$(3.7 \pm 0.5) \times 10^{-5}$ s^{-1}] corresponds to the heme dissociation rate from H39L. On the other hand, the absorption change after mixing CN-H63L and apomyoglobin is biphasic, having a fast phase with a rate of 0.020 ± 0.004 s^{-1} and a slow phase with a rate of $(6.0 \pm 1.1) \times 10^{-4}$ s^{-1} (data not shown). Hargrove et al. (*50*) reported that dicyanohemin binding to apomyoglobin is a first-order process with a rate constant of 0.019 s^{-1}, which coincides with the rate of the fast phase in our observation. We conclude that the fast phase observed in the reaction of CN-H63L corresponds to the incorporation of free heme into apomyoglobin and the slow phase to the heme dissociation from H63L. This observation indicates that CN-H63L is actually in the mixture of free heme and the heme-bound protein. The amplitude of the fast phase is ca. 10%, which is consistent with the suggestion that the slightly reduced Soret absorption of CN-H63L (Figure 1) is due to the equilibrium between the holo form and free heme.

To summarize the results described above, the heme association of the H39L mutant is 1.8 times faster than that of the H63L mutant, and the heme dissociation of H39L is 16 times slower than that of H63L. The equilibrium association constants of the heme with the mutants calculated using the rates of the heme dissociation and association are 7.3×10^4 and 2.5×10^3 mM^{-1} for H39L and H63L, respectively. We conclude that the complex between the loop containing His63 and heme is more stabilized than that between the loop containing His39 and heme.

Heme Incorporation of Wild-Type Cyt b_5 Monitored by Electronic Absorption Spectroscopy. We have shown that the loop containing His63 has a higher affinity for heme. To confirm the properties of the loops in the wild-type protein, the kinetic process of the heme incorporation into wild-type cyt b_5 was investigated using rapid-scan absorption measurements. A typical example of the kinetic absorption spectra is presented in Figure 3, which was obtained after mixing hemin dicyanide with wild-type apocyt b_5 to final concentrations of 1 and 5 μM, respectively, in the presence of 25 mM cyanide. The shift of the Soret absorption band without isosbestic points was observed, which indicates the existence of transient components that have absorption spectra that are different from those of bis-cyanide- and bis-histidine-coordinated hemes.

The coordination structure of the transient components can be assumed to be the CN-His form, since the absorption spectrum at 5 s possesses a Soret maximum at 418 nm (Figure 3) that is similar to those of the CN-H39L and CN-H63L mutants (419 nm) (Figure 1). If the assumption is correct, all the rapid-scan spectra recorded during the incorporation process should be the superposition of the three spectra of bis-cyanide-coordinated heme (bis-CN), wild-type holocyt b_5 (bis-His), and the CN-His form of the heme.

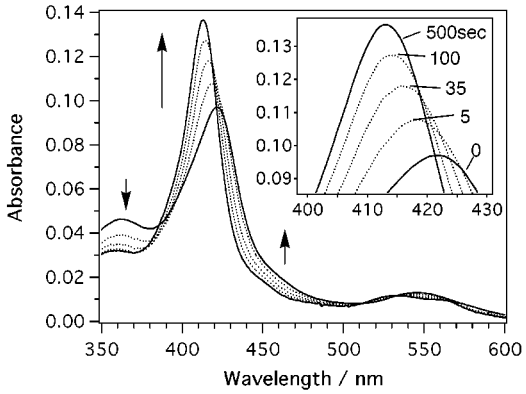

FIGURE 3: Rapid-scan optical absorption spectra during the heme incorporation process of apocyt b_5. Hemin dicyanide and apocyt b_5 were rapidly mixed to final concentrations of 1 and 5 μM, respectively, and the following process of heme incorporation was observed from 0 to 500 s. The buffer solution contained 25 mM NaCN. The inset shows the expansion of the Soret region.

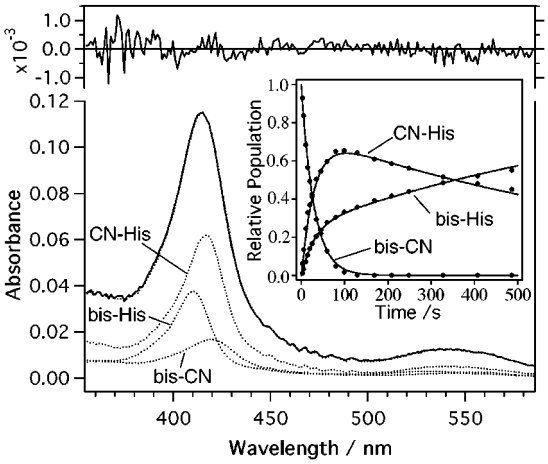

FIGURE 4: Typical example of the deconvolution of the rapid-scan absorption spectrum. The solid line in the main panel indicates the transient spectrum obtained 30 s after the initiation of the heme incorporation into wild-type cyt b_5. The spectrum was deconvoluted using the standard spectra of bis-CN, CN-His (CN-H39L), and bis-His, whose relative contributions are 27, 55, and 18%, respectively. The dotted lines indicate the three standard spectra used for the deconvolution. The residuals of the deconvolution are shown on the top. The inset shows time-dependent changes in the populations of bis-CN, CN-His, and bis-His. The points are the experimental data obtained from the deconvolution of the rapid-scan spectra. The solid lines are the simulated fits to the observed population changes using the simplified misfold model presented inside the broken box in Scheme 3. The estimated values of k_1, k_3, and k_2/k_4 are 0.038 s^{-1}, 0.0040 s^{-1}, and 2.1, respectively.

Therefore, the observed rapid-scan spectra were deconvoluted using the three standard spectra of bis-CN, bis-His, and CN-H39L. Since the H39L mutant forms a stoichiometric complex with heme, its absorption spectrum is appropriate for CN-His. A representative example of the deconvolution using the three spectra is shown in Figure 4, in which bis-CN, bis-His, and CN-His are estimated to contribute 27, 18, and 55% of the total population, respectively. The residuals of the fitting were within the experimental error for all the rapid-scan spectra obtained from 0 to 500 s. The time-dependent changes of the three populations during the heme association process are plotted in the inset of Figure 4. We conclude that the kinetic process of heme incorporation into wild-type cyt b_5 involves the transient components whose coordination structure is the His-CN form.

Heme Incorporation of Mutant and Wild-Type Cyt b_5s Monitored by CD Spectroscopy. The rapid-scan absorption measurements revealed that the kinetic process of the heme incorporation into wild-type cyt b_5 involves the transient components whose coordination structure is the His-CN form. The axial histidine of the heme in the transient components should be either His39, His63, or histidines on the protein surface. Since the CD spectra in the Soret region of H39L and H63L are distinct as shown in Figure 2, we can identify the axial ligand by observing the kinetic CD spectra for the heme incorporation process of apocyt b_5.

We first observed the heme incorporation processes of mutant cyt b_5s. The time-dependent changes in the Soret ellipticities were obtained after mixing mutant apocyt b_5s and hemin dicyanide to final concentrations of 5 and 1 μM, respectively, in the presence of 25 mM cyanide (data not shown). The observed CD changes in the Soret region were well-correlated with the absorbance changes. The CD value of H39L decreased single-exponentially with the rate constant of 0.017 ± 0.003 s^{-1} (0.015 ± 0.001 s^{-1} from the optical data). The CD value of H63L increased single-exponentially with the rate constant of 0.0071 ± 0.002 s^{-1} (0.0090 ± 0.0005 s^{-1} from the optical data). These results indicate that the complex formations simultaneously induce the changes in the optical absorption and the optical ellipticity of the heme. Since a heme randomly attached on the protein surface affords no ellipticity, the coordination of surface histidines is unlikely to occur in the heme association processes of mutant cyt b_5s.

The CD spectral changes during the heme incorporation process of wild-type cyt b_5 were followed by monitoring the time courses of the optical ellipticities at every 1 nm between 412 and 428 nm. The obtained data set is presented as the time-resolved spectra at several duration times (Figure 5A). The CD spectra obtained from 30 to 706 s show that the initial negative peaks around 422 nm shift to 418 nm as the reaction proceeds. Assuming that the CN-His39- and CN-His63-coordinated states of wild-type cyt b_5 exhibit CD spectra that are similar to those of the corresponding mutants of cyt b_5, we deconvoluted the observed CD spectra using the standard CD spectra of wild-type cyt b_5, CN-H39L and CN-H63L.[2] As shown in Figure 5B, the time courses of the populations of CN-His39, CN-His63, and bis-His coincide well with those obtained from the optical absorption data (Figure 4, inset). Both CN-His39 and CN-His63 are present at a ratio of 1:5 to 1:6, and the levels decrease with almost the same rate. These results demonstrate that the transient components observed in the heme incorporation into wild-type cyt b_5 are the mixture of the two coordination states, but the major component is CN-His63.

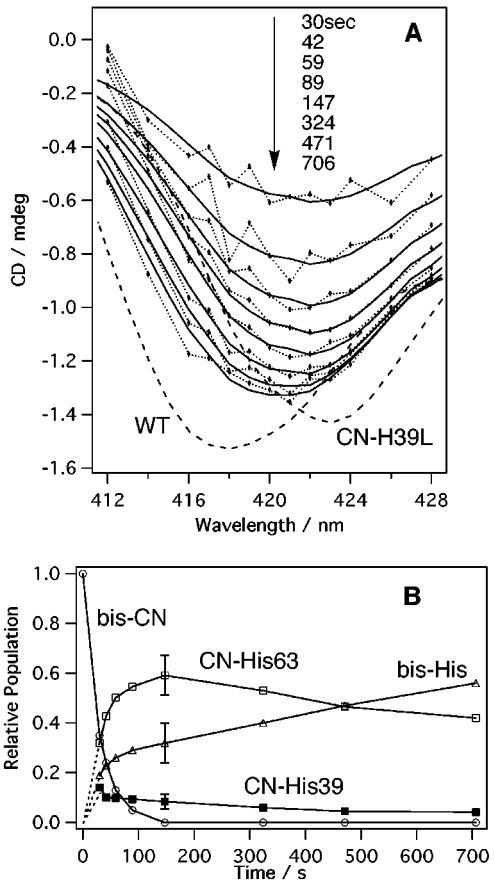

FIGURE 5: (A) Time-dependent CD spectra during the heme incorporation process of apocyt b_5. Hemin dicyanide and apocyt b_5 were mixed to final concentrations of 1 and 5 μM, respectively, in the presence of 25 mM NaCN, and the following heme incorporation was monitored at fixed wavelengths. The points indicate the observed CD values at 30, 42, 59, 89, 147, 324, 471, and 706 s after initiation of the reaction. The broken lines represent the standard CD spectra of the wild type and CN-H39L. The solid lines are the results of the fitting to the data using the standard spectra of the wild type, CN-H39L, and CN-H63L. The populations of bis-CN were fixed to the values estimated from the optical data. (B) Time-dependent changes in the populations of bis-CN (○), bis-His (△), CN-His39 (■), and CN-His63 (□) determined by the fitting to the transient CD spectra.

DISCUSSION

Stability of the Heme−Mutant Associations. We constructed two mutants of cyt b_5 to differentiate the roles of the two heme-binding loops. The spectroscopic properties of the constructed mutants, H39L and H63L, in the presence of cyanide indicate that heme is incorporated inside the pockets with histidine and cyanide as the axial ligands. Sligar and his collaborators reported that the substitution of His63 with alanine (H63A) disintegrates the heme pocket due to the small volume of the alanine side chain that allows the penetration of water molecules (*40*). In contrast, both of the current mutants are stable in the cyanide-bound form, probably because of the similarity in the side chain volumes of leucine and histidine. The hydrophobic property of leucine might also help the mutants exclude water molecules from the pockets. We, therefore, consider that the current mutants possess the heme pockets whose structures are similar to that of wild-type cyt b_5. We can expect that the spectroscopic properties of the mutants would mimic those of the transient components observed in the heme incorporation process of wild-type cyt b_5, and that the kinetic properties of the mutants would reflect the heme binding properties of the remaining loops.

We first investigated the heme incorporation and dissociation kinetics of the mutants. It was demonstrated that the heme association rate of H39L at pH 8.0 (2.7 ± 0.2 mM^{-1} s^{-1}) is 1.8 times larger than that of H63L (1.5 ± 0.1 mM^{-1}

[2] Since the solution that gave the CD spectrum of CN-H63L (Figure 2) actually included ~10% free heme, we multiplied the CD spectrum by 1.1 and used it as the standard CD spectrum of CN-His39.

Scheme 1

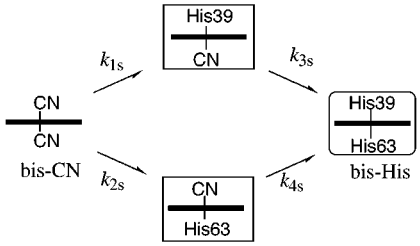

Scheme 2

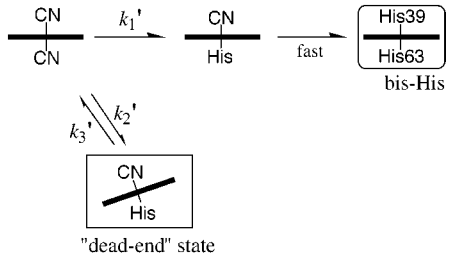

s^{-1}). The faster association of H39L is also observed at pH 9.0, which is much larger than the normal pK_a value of histidine (6.3−6.6). Thus, the possible difference in the ionization state of the axial histidines at pH 8.0 is not responsible for the difference in the association constants. We next observed that the heme dissociation rate from H63L [$(6.0 \pm 1.1) \times 10^{-4}$ s^{-1}] is 16 times larger than that from H39L [$(3.7 \pm 0.5) \times 10^{-5}$ s^{-1}]. The overall equilibrium association constant for association of heme with H39L is 29 times larger than that with H63L. Since the region around His63 of apocyt b_5 shows a larger fluctuation compared to the region around His39 (*24*, *25*), we conclude that the fluctuating loop possesses a significantly higher affinity for heme. It should be noted that the difference in the two loops is more prominently reflected in the dissociation constants than in the association constants.

Pathway of Heme Incorporation into Wild-Type Cyt b_5. To ascertain the importance of the His63 loop in heme binding, we investigated the functions of the two loops in the heme association process of wild-type cyt b_5. We clarified that the process involves the transient components whose coordination structure is the CN-His form. The kinetic CD spectroscopy indicated that the dominant part of the transient components possesses His63 as the axial ligand. However, we cannot distinguish whether the His63-coordinated component is the obligate intermediate for the heme incorporation as shown in Scheme 1 or the dead-end state that traps the incorporation as shown in Scheme 2. If the latter mechanism is correct, we should consider that the His63 loop retards the heme association process. It is important to establish the mechanism of the heme incorporation in an effort to understand the functions of the loops.

We presented the time courses of bis-His, bis-CN, CN-His39, and CN-His63 in the inset of Figure 4 and in panel B of Figure 5, which indicate the presence of two kinetic phases. In the first phase, the levels of bis-His, CN-His63, and CN-His39 build up rapidly with the depletion of the bis-CN level. In the second phase, the level of bis-His slowly increases, accompanied by decreases in the levels of CN-His39 and CN-His63. These features are different from those expected from the "parallel sequential model" depicted in

Scheme 3

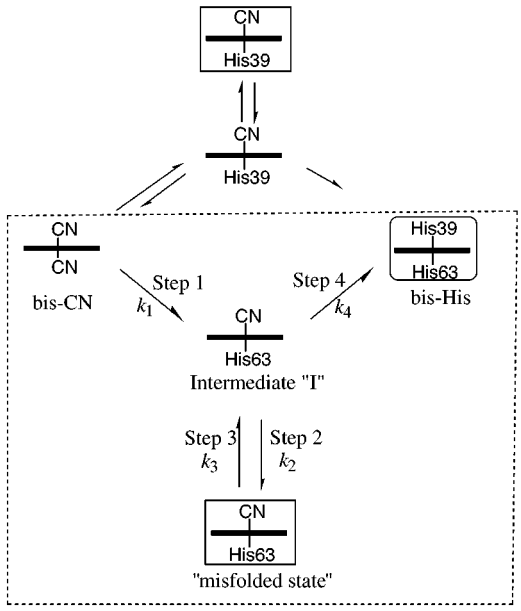

Scheme 1. If the sequential model is correct, the rise of the intermediate should precede the increase in the level of the product. The simultaneous increases in CN-His39, CN-His63, and bis-His levels in the first phase (Figure 5B) contradict the model. Furthermore, we cannot reproduce the time courses of either CN-His39 or CN-His63 using the sequential model with any combination of the kinetic rate constants ($k_{1s} \sim k_{4s}$ in Scheme 1). We conclude that both of the CN-His components are not obligatory.

We next discuss the possibility of the "dead-end model" shown in Scheme 2. The model considers that the observed CN-His components represent the trapped states with His63, His39, or surface histidines as the axial ligand. We can rule out the heme trapping at the surface histidines, since no trapping effect was observed in the heme incorporation processes of the mutants. The heme trapping at His63 can also be neglected, since the rate of hemin dissociation from the H39L mutant (3.7×10^{-5} s^{-1}) is much slower than the observed slow phase of the wild-type protein ($\sim 10^{-3}$ s^{-1}). Furthermore, the examination of the cyanide concentration dependency of the rate constants ($k_1' \sim k_3'$) estimated using the model contradict the predictions of the model.[3] We therefore consider that the major intermediate, CN-His63, is not the "dead-end state".

We propose the "misfold model" shown in Scheme 3 to explain the observed kinetics. The model considers the transient CN-His components as the misfolded states, which possess either His39 or His63 as the axial ligand and are in equilibrium with the obligate intermediates. The misfolded state and the obligate intermediate that are in equilibrium possess the same heme coordination structure but different protein conformations. The misfolded states and the product

[3] The dead-end model predicts that the values of k_1' and k_2' are inversely proportional to the cyanide concentration, since these processes contain the competition between cyanide and axial histidines. However, the values of $1/k_1'$ and $1/k_2'$ estimated using the model and experimental data presented in Figure 6 are not proportional to the cyanide concentration (data not shown). Thus, the dead-end model cannot consistently describe the kinetic results of the major CN-His63 component in the observed concentration range of cyanide.

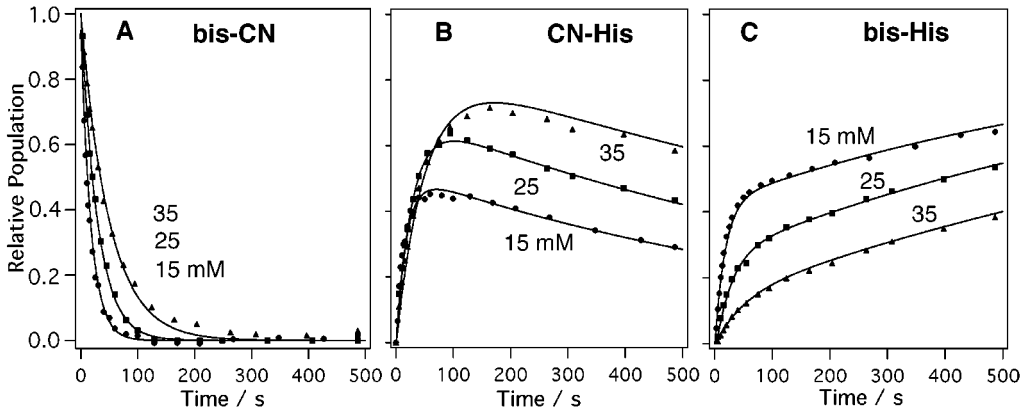

FIGURE 6: Time-dependent changes in the populations of bis-CN (A), CN-His (B), and bis-His (C) during the heme incorporation into apocyt b_5 conducted under different CN concentrations. Concentrations of apoprotein and dicyanohemin after the mixing were 5 and 1 μM, respectively. Three cyanide concentrations, 15 (●), 25 (■), and 35 mM (▲), were investigated. The solid lines are the best-fit simulation to the data using the simplified misfold model presented inside the broken box in Scheme 3.

are formed competitively from the obligate intermediates. While we consider that the model is necessary to explain the time dependencies of both CN-His39 and CN-His63, it possesses too many rate constants to be determined uniquely. We therefore ignored the contribution of the minor intermediate, CN-His39, in establishing the major pathway of heme incorporation. The simplified misfold model is depicted inside the broken box in Scheme 3. The rate constants estimated using the simplified model appear to exhibit minor deviations caused by neglecting CN-His39. However, the quantitative analysis using the simplified model should reveal the roles of CN-His63 that amounts to more than 80% of the transient components.

The simplified misfold model has two kinds of transient components, I and misfolded state, and four rate constants, k_1-k_4. We ignored the back reaction from I to bis-CN due to the slow rate of dissociation of heme from CN-H39L (3.7×10^{-5} s^{-1}) compared to the rate of the heme incorporation into the wild-type protein ($10^{-3}-10^{-2}$ s^{-1}). As shown in the inset of Figure 4, the model can reproduce the observed kinetic trace of each component and gives rate constants k_1 and k_3 and a ratio of the rate constants, k_2/k_4. To verify the simplified misfold model, we will demonstrate that the model consistently describes the cyanide and apoprotein concentration dependencies of the estimated rate constants. Step 1 of the model includes the dissociation of cyanide from dicyanohemin followed by the coordination of the axial histidine to the open coordination site of monocyanohemin. Since monocyanohemin can bind both cyanide and apoprotein, k_1 is expected to increase linearly with the apoprotein concentration and with the inverse of the cyanide concentration. Steps 2 and 3 involve only the conformational transitions of the protein, and should be independent of the apoprotein and cyanide concentrations. Step 4 involves the dissociation of cyanide, and should be dependent on the cyanide concentration, but independent of the apoprotein concentration. These predictions from the simplified misfold model can be experimentally verified.

We first examined the cyanide concentration dependencies of k_1-k_4. Apoprotein and dicyanohemin solutions were mixed to final concentrations of 5 and 1 μM, respectively, under three cyanide concentrations (15, 25, and 35 mM). The time courses of bis-CN, bis-His, and CN-His were determined by the deconvolution of the rapid-scan absorption spectra, and were plotted in the panels A−C of Figure 6, respectively. The best-fit rate constants (k_1, k_3, and k_2/k_4) were evaluated by fitting the obtained time courses using the simplified misfold model. As shown in panel A of Figure 7, while $1/k_1$ and k_2/k_4 are proportional to the cyanide concentration, k_3 is independent of the cyanide concentration. We next examined the apoprotein concentration dependencies of k_1-k_4. Apoprotein solutions at concentrations of 3, 5, 10, and 15 μM were allowed to react with 1 μM dicyanohemin in the presence of 25 mM cyanide (data not shown). Rate constants were analyzed and presented in panel B of Figure 7, which indicates that k_1 is proportional to the apoprotein concentration and that k_2/k_4 and k_3 show no change. All these observations are consistent with the predictions from the simplified model. We conclude that the simplified misfold model can consistently describe the major pathway of heme incorporation of cyt b_5.

The simplified misfold model ignores the minor contribution of CN-His39. Since the observed CN-His39 component cannot be the on-pathway intermediate as judged from its time dependency, we propose that CN-His39 might be either the misfolded state or the trapped state. Scheme 3 can express both of the cases by a proper choice of rate constants. Unfortunately, it is impractical to establish the pathway involving CN-His39 due to the uncertainty in the estimated amount of the minor CN-His39 component. We conclude, however, that the heme incorporation process of cyt b_5 proceeds through the two pathways, and that the dominant pathway involves the initial coordination of His63. We confirmed that the loop containing His63 captures heme faster than the other loop in both wild-type and mutant cyt b_5s.

Identification of the Step That Involves the Folding of the Fluctuating Loop. We revealed that the fluctuating loop containing His63 can form the stabilized heme−loop complex. To characterize the mechanism of stabilization, we investigated the urea concentration dependency of the heme incorporation process. Since urea is known to disturb hydrophobic interaction of proteins (*51*, *52*), the processes that involve the folding of protein backbones should be decelerated by increasing the urea concentration.

The heme incorporation experiments under various urea concentrations from 0 to 1.5 M were conducted. The rapid-scan absorption spectra were deconvoluted using the spectra

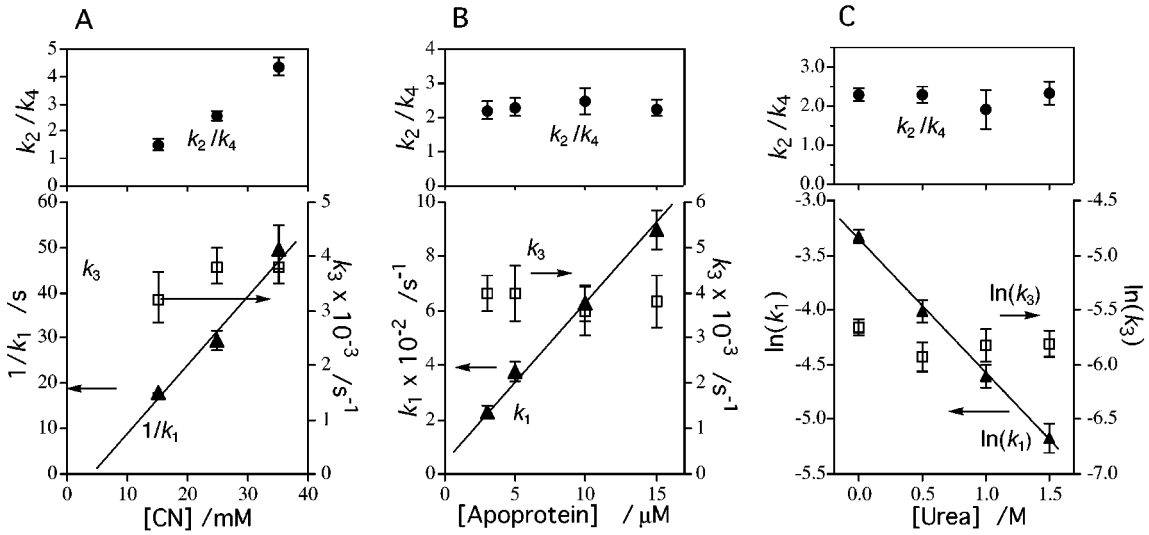

FIGURE 7: Dependence of k_1, k_3, and k_2/k_4 on the cyanide (A), apoprotein (B), and urea (C) concentrations. Black triangles, white squares, and black circles denote the values of k_1, k_3, and k_2/k_4, respectively, that were obtained by fitting the experimental data using the simplified misfold model presented inside the broken box in Scheme 3.

of bis-CN, bis-His, and CN-H39L measured at respective urea concentrations (data not shown). The resultant time courses of the three components were fitted using the simplified misfold model to estimate the rate constants. It is apparent that while the observed k_3 and k_2/k_4 values are constant, the ln(k_1) value decreases linearly with the urea concentration (panel C of Figure 7). The urea dependency of k_1 demonstrates that the transition state for step 1 possesses the folded backbone structure. The constant behavior of k_3 and k_2/k_4 suggests that forward and backward transitions between I and the misfolded state (steps 2 and 3) and the transition from I to the native state (step 4) are associated with only a small amount of the backbone folding.[4] We note that the experiments were conducted at relatively low urea concentrations (<1.5 M). Since the midpoint urea concentration for the equilibrium unfolding of apocyt b_5 is ca. 2 M (M. Ihara et al., unpublished), the amount of the unfolded state of apocyt b_5 is small. The liner concentration dependency of the estimated kinetic constants also supports the kinetic scheme without the unfolded state of apocyt b_5.[5]

We can roughly estimate the amount of backbone folding in step 1 from its urea concentration dependency. The values of ln(k_1) conform to eq 1:

$$\ln(k_1) = \ln(k_1^{H_2O}) + m_{1f}[\text{urea}] \quad (1)$$

where $k_1^{H_2O}$ is the rate constant in the absence of urea and m_{1f} is the slope of the plot. The m value is known to be proportional to the difference in the solvent accessible surface area (ΔASA) between the initial and transition states (*53*). According to the empirical relationship between m and ΔASA derived by Myers et al. (*53*), the observed m_{1f} value ($m_{1f}RT = 650$ cal mol^{-1} M^{-1})[6] corresponds to a ΔASA of ca. 2500 ± 1000 Å^2. The theoretical ΔASA between the holo and apo forms of cyt b_5 is ca. 1900 Å^2, estimated using the program ACCESS (*54*) and coordinate data of cyt b_5 (*33*) and heme. Considering the large uncertainty in the empirical relationship by Myers et al. (*53*),[7] we consider that the two values are comparable. We conclude that a large part of the fluctuating loop in apocyt b_5 is already folded at the transition state of step 1. The result demonstrates that the first step of the heme incorporation is associated with the folding of the loop containing His63.

Roles of the Fluctuating Loops in Heme-Binding Proteins. We revealed that the fluctuating loop containing His63 exhibits a faster heme association and a slower heme dissociation compared to those of the other loop containing His39. The difference is more pronounced in the dissociation process. The previous calorimetric study on apocyt b_5 indicated that apocyt b_5 is entropically unfavorable compared to holocyt b_5, indicating that parts of nonpolar residues, being buried in holocyt b_5, are exposed to the solvent in apocyt b_5 (*55*, *56*). The urea concentration dependency of k_1 also suggests that a considerable amount of hydrophobic interaction is established in step 1. We infer that the affinity of the His63 loop for heme might be ascribed to extensive hydrophobic contacts between the loop and heme.

A careful inspection of the X-ray structure of cyt b_5 allows us to notice that the backbone structures of the two loops differ in the extent of packing between the heme and loops. As shown in Figure 8 (*37*), the His39 loop in the holo form possesses a hydrophobic cluster tightly packed by three leucines, Leu32, -36, and -46, which is also present in the apo structure (*24*, *25*). On the contrary, the two terminals of the His63 loop are separated from each other. The two helices of the His63 loop possess no direct interaction except for one hydrogen bond between Arg68 and Glu59. The weak

[4] The small difference in the amount of backbone folding between the misfolded state and I suggests that the two states possess similar conformations. We propose that His39 might form a hydrogen bond with the axial cyanide in the misfolded state but not in I.

[5] Urea might also modulate the structure of the transition state for step 1 that could complicate our analysis. We presume the effect can be ignored due to the relatively low urea concentrations (<1.5 M) used in our experiments and the observed linearity of the ln(k_1) versus [urea] plot (panel C of Figure 7).

[6] Myers et al. (*53*) defined the m (cal mol^{-1} M^{-1}) values from the equilibrium experiments. The m_{1f} (M^{-1}) values obtained in our kinetic experiments must be multiplied by RT to match the units.

[7] The correlation coefficient between m and ΔASA estimated by Myers et al. (*53*) is rather small ($R = 0.84$).

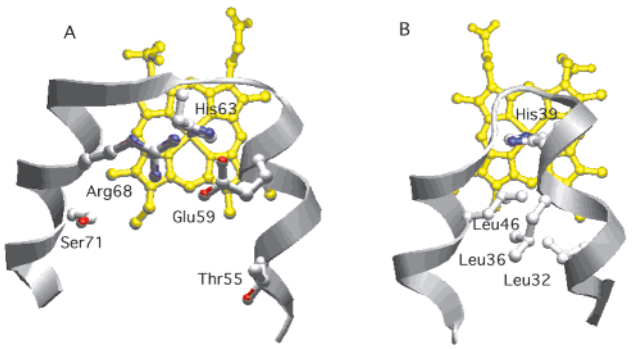

FIGURE 8: (A) Local structure of the loop including His63 in the holo form of cyt b_5. The region between Asp53 and Tyr74 is presented. Thr55, Glu59, His63, Arg68, Ser71, and heme are shown as a ball-and-stick model. (B) The local structure of the loop including His39 in the holo form of cyt b_5. The region between Asp31 and Gly51 is presented. Lue32, Lue36, His39, Lue46, and heme are shown as a ball-and-stick model. The figures were prepared using the program Swiss-PdbViewer (*69*).

interaction within the His63 loop would induce the fluctuation in the apo form, but enables a larger contact between the loop and heme. The loop from Gly52 to Tyr74 has a larger contact area with heme (ca. 350 Å^2) than the loop from Leu32 to Gly51 (ca. 275 Å^2). We find that the larger equilibrium association constant for the H39L−heme complex would mainly be ascribed to the larger heme−protein contact of the His63 loop.

A folding of the backbone structure in the heme-binding step also is observed for myoglobin. Previous studies clarified that apomyoglobin incorporates dicyanohemin inside the pocket in the first step and displaces one of the axial cyanides with the proximal histidine in the second step (*50*, *57*). The formation of the secondary structures corresponding to the folding of the fluctuating proximal loop (*15*−*18*) is associated with the first step. Thus, while the timings of the histidine coordination are different between cyt b_5 and myoglobin, both proteins exhibit the folding of the heme-binding loop and the incorporation of the heme simultaneously. We suggest that the importance of the fluctuating loop in the stable heme binding might be a general observation.

Several recent studies indicated the importance of the disordered loops for substrate (*58*, *59*), DNA (*60*, *61*), and metal (*62*, *63*) binding, and suggested the protein design using the loops. We also propose that the artificial design of stable heme-binding proteins, including five-coordinate hemes, might become possible by using the fluctuating heme-binding loops. In support of this expectation, we found that while H63L is unstable in the absence of cyanide, H39L forms a stable aquomet structure at 10 °C (M. Ihara et al., submitted). Another interesting observation is that the folded structure of the His63 loop is similar to that of the proximal loops of globins (*64*−*66*). Furthermore, we have replaced the proximal loop of myoglobin, which is termed the "heme-binding module", with that of hemoglobin without causing a severe destabilization of the protein structure (*67*, *68*). The fluctuating loop for the heme-binding might be an important construction block of natural and artificial heme proteins.

CONCLUSION

We demonstrated that the process of heme incorporation into the apo form of cyt b_5 proceeds through the two pathways and that the dominant pathway involves the initial coordination of His63. The fluctuating loop containing His63 captures heme faster than the other loop containing His39, and makes the more stabilized complex. Since the His63 loop possesses a larger heme−loop contact in the holo form compared to the other loop, we suggest that the fluctuation might be important in attaining the larger hydrophobic interaction between heme and the loop. The finding would be important for the artificial designs of proteins that can bind heme and other substrates.

ACKNOWLEDGMENT

We are grateful to Prof. S. G. Sligar (University of Illinois, Urbana, IL) for a gift of the expression vector containing the rat cytochrome b_5 gene. We thank the referees for fruitful suggestions for improving the manuscript.

REFERENCES

1. Antonini, M., and Brunori, E. (1971) in *Hemoglobin and myoglobin in their reactions with ligands* (Neuberger, A., and Tatum, E. L., Eds.) North-Holland Publishers, Amsterdam.
2. Lemberg, R., and Barrett, J. (1973) *Cytochromes*, Academic Press, New York.
3. Scheer, H. (1991) *Chlorophylls*, CRC Press, Boca Raton, FL.
4. Rodgers, K. R. (1999) *Curr. Opin. Chem. Biol. 3*, 158−167.
5. Choma, C. T., Lear, J. D., Nelson, M. J., Dutton, P. L., Robertson, D. E., and DeGrado, W. F. (1994) *J. Am. Chem. Soc. 116*, 856−865.
6. Robertson, D. E., Farid, R. S., Moser, C. C., Urbauer, J. L., Mulholland, S. E., Pidikiti, R., Lear, J. D., Wand, A. J., DeGrado, W. F., and Dutton, P. L. (1994) *Nature 368*, 425−432.
7. Rabanal, F., DeGrado, W. F., and Dutton, P. L. (1996) *J. Am. Chem. Soc. 118*, 473−474.
8. Kalsbeck, W. A., Robertson, D. E., Pandey, R. K., Smith, K. M., Dutton, P. L., and Bocian, D. F. (1996) *Biochemistry 35*, 3429−3438.
9. Gibney, B. R., Rabanal, F., Skalicky, J. J., Wand, A. J., and Dutton, P. L. (1997) *J. Am. Chem. Soc. 119*, 2323−2324.
10. Rojas, N. R., Kamtekar, S., Simons, C. T., McLean, J. E., Vogel, K. M., Spiro, T. G., Farid, R. S., and Hecht, M. H. (1997) *Protein Sci. 6*, 2512−2524.
11. Gibney, B. R., Rabanal, F., Reddy, K. S., and Dutton, P. L. (1998) *Biochemistry 37*, 4635−4643.
12. Sharp, R. E., Moser, C. C., Rabanal, F., and Dutton, P. L. (1998) *Proc. Natl. Acad. Sci. U.S.A. 95*, 10465−10470.
13. Shifman, J. M., Moser, C. C., Kalsbeck, W. A., Bocian, D. F., and Dutton, P. L. (1998) *Biochemistry 37*, 16815−16827.
14. Gibney, B. R., and Dutton, P. L. (1999) *Protein Sci. 8*, 1888−1898.
15. Eliezer, D., and Wright, P. E. (1996) *J. Mol. Biol. 263*, 531−538.
16. Eliezer, D., Jennings, P. A., Dyson, H. J., and Wright, P. E. (1997) *FEBS Lett. 417*, 92−96.
17. Eliezer, D., Yao, J., Dyson, H. J., and Wright, P. E. (1998) *Nat. Struct. Biol. 52*, 148−155.
18. Lecomte, J. T., Sukits, S. F., Bhattacharya, S., and Falzone, C. J. (1999) *Protein Sci. 8*, 1484−1491.
19. Feng, Y., Sligar, G., and Wand, A. J. (1994) *Nat. Struct. Biol. 1*, 30−35.
20. Laidig, K. E., and Daggett, V. (1996) *Folding Des. 1*, 335−346.
21. Fuentes, E. J., and Wand, A. J. (1998) *Biochemistry 37*, 3687−3698.
22. Moore, C. D., al-Misky, O. N., and Lecomte, J. T. (1991) *Biochemistry 30*, 8357−8365.
23. Moore, C. D., and Lecomte, J. T. (1993) *Biochemistry 32*, 199−207.
24. Falzone, C. J., Mayer, M. R., Whiteman, E. L., Moore, C. D., and Lecomte, J. T. (1996) *Biochemistry 35*, 6519−6526.

25. Bhattacharya, S., Falzone, C. J., and Lecomte, J. T. (1999) *Biochemistry 38*, 2577−2589.
26. Tainer, J. A., Getzoff, E. D., Alexander, H., Houghten, R. A., Olson, A. J., Lerner, R. A., and Hendrickson, W. A. (1984) *Nature 312*, 127−134.
27. Lefevre, J. F., Dayie, K. T., Peng, J. W., and Wagner, G. (1996) *Biochemistry 35*, 2674−2686.
28. Hodsdon, M. E., and Cistola, D. P. (1997) *Biochemistry 36*, 2278−2290.
29. Strittmatter, P., Spatz, L., Corcoran, D., Rogers, M. J., Setlow, B., and Redline, R. (1974) *Proc. Natl. Acad. Sci. U.S.A. 71*, 4565−4569.
30. Tamburini, P. P., White, R. E., and Schenkman, J. B. (1985) *J. Biol. Chem. 260*, 4007−4015.
31. Hultquist, D. E., and Passon, P. G. (1971) *Nat. New Biol. 229*, 252−254.
32. Cohen, B., and Estabrool, R. W. (1971) *Arch. Biochem. Biophys. 143*, 54−65.
33. Mathews, F. S., Argos, P., and Levine, M. (1972) *Cold Spring Harbor Symp. Quant. Biol. 36*, 387−393.
34. Durley, R. C. E., and Mathews, F. S. (1996) *Acta Crystallogr. D52*, 65−76.
35. Muskett, F. W., Kelly, G. P., and Whitford, D. (1996) *J. Mol. Biol. 258*, 172−189.
36. Banci, L., Bertini, I., Ferroni, F., and Rosato, A. (1997) *Eur. J. Biochem. 249*, 270−279.
37. Arnesano, F., Banci, L., Bertini, I., and Felli, I. C. (1998) *Biochemistry 37*, 173−184.
38. Arnesano, F., Banci, L., Bertini, I., Felli, I. C., and Koulouglioti-otis, D. (1999) *Eur. J. Biochem. 260*, 347−354.
39. Banci, L., Bertini, I., Rosato, A., and Scacchieri, S. (2000) *Eur. J. Biochem. 267*, 755−766.
40. Beck von Bodman, S., Schuler, M. A., Jollie, D. R., and Sligar, S. G. (1986) *Proc. Natl. Acad. Sci. U.S.A. 83*, 9443−9447.
41. Paul, K. G., Theorell, H., and Akeson, A. (1953) *Acta Chem. Scand. 7*, 1284−1287.
42. Teale, F. W. J. (1959) *Biochim. Biophys. Acta 35*, 543.
43. Strittmatter, P. (1960) *J. Biol. Chem. 235*, 2492−2497.
44. Qian, W., Sun, Y. L., Wang, Y. H., Zhuang, J. H., Xie, Y., and Huang, Z. X. (1998) *Biochemistry 37*, 14137−14150.
45. Hargrove, M. S., Singleton, E. W., Quillin, M. L., Ortiz, L. A., Phillips, G. N., Jr., Olson, J. S., and Mathews, A. J. (1994) *J. Biol. Chem. 269*, 4207−4214.
46. Hsu, M. C., and Woody, R. W. (1971) *J. Am. Chem. Soc. 93*, 3515−3524.
47. Gruenke, L. D., Sun, J., Loehr, T. M., and Waskell, L. (1997) *Biochemistry 36*, 7114−7125.
48. Hunter, C. L., Lloyd, E., Eltis, L. D., Rafferty, S. P., Lee, H., Smith, M., and Mauk, A. G. (1997) *Biochemistry 36*, 1010−1017.
49. Hargrove, M. S., Wilkinson, A. J., and Olson, J. S. (1996) *Biochemistry 35*, 11300−11309.
50. Hargrove, M. S., Barrick, D., and Olson, J. S. (1996) *Biochemistry 35*, 11293−11299.
51. Tanford, C. (1968) *Adv. Protein Chem. 23*, 132−282.
52. Pace, C. N. (1986) *Methods Enzymol. 131*, 266−279.
53. Myers, J. K., Pace, C. N., and Scholtz, J. M. (1995) *Protein Sci. 4*, 2138−2148.
54. Lee, B., and Richards, F. M. (1971) *J. Mol. Biol. 55*, 379−400.
55. Pfeil, W. (1993) *Protein Sci. 2*, 1497−1501.
56. Manyusa, S., and Whitford, D. (1999) *Biochemistry 38*, 9533−9540.
57. Kawamura-Konishi, Y., Kihara, H., and Suzuki, H. (1988) *Eur. J. Biochem. 170*, 589−595.
58. Freitag, S., Le Trong, I., Klumb, L., Stayton, P. S., and Stenkamp, R. E. (1997) *Protein Sci. 6*, 1157−1166.
59. Quirk, P. G., Smith, K. J., Thomas, C. M., and Jackson, J. B. (1990) *Biochim. Biophys. Acta 1412*, 139−148.
60. Markus, M. A., Hinck, A. P., Huang, S., Draper, D. E., and Torchia, D. A. (1997) *Nat. Struct. Biol. 4*, 70−77.
61. Dekker, J., Kanellopoulos, P. N., van Oosterhout, J. A., Stier, G., Tucker, P. A., and van der Vliet, P. C. (1998) *J. Mol. Biol. 277*, 825−838.
62. Tuzi, S., Yamaguchi, S., Tanio, M., Konishi, H., Inoue, S., Naito, A., Needleman, R., Lanyi, J. K., and Saito, H. (1999) *Biophys. J. 76*, 1523−1531.
63. Akke, M., Skelton, N. J., Kordel, J., Palmer, A. G., III, and Chazin, W. J. (1993) *Biochemistry 32*, 9832−9844.
64. Argos, P., and Rossmann, M. G. (1979) *Biochemistry 18*, 4951−4960.
65. Mathews, F. S., Czerwinski, E. W., and Argos, P. (1979) *The porphyrins*, Vol. 3, pp 107−147, Academic Press, New York.
66. Blake, C. C. F. (1981) *Nature 291*, 616.
67. Inaba, K., Ishimori, K., Imai, K., and Morishima, I. (1998) *J. Biol. Chem. 273*, 8080−8087.
68. Inaba, K., Ishimori, K., and Morishima, I. (1998) *J. Mol. Biol. 283*, 311−327.
69. Guex, N. (1996) *Experientia 52*, A26.

BI9922289